Open Ceramics 16 (2023) 100449

Contents lists available at ScienceDirect

Open Ceramics

journal homepage: www.sciencedirect.com/journal/open-ceramics

On the structure of Ag-containing sol-gel bioactive glasses: A surface crystal growth of metallic silver removes its network modifier role in the glass structure

Roger Borges [a,b], Juliana S.S. Oliveira [a], Antônia P. Queiroz [a], Telma Zambanini [a], Akiko M. Hanashiro [a], Nelson B. Lima [c], José F. Schneider [d], Juliana Marchi [a,*]

[a] Centro de Ciências Naturais e Humanas, Universidade Federal do ABC, Santo André, SP, Brazil
[b] School of Biomedical Engineering, Faculdade Israelita de Ciências da Saúde Albert Einstein, Hospital Israelita Albert Einstein, São Paulo, SP, Brazil
[c] Centro de Ciência e Tecnologia dos Materiais, Instituto de Pesquisas Energéticas e Nucleares, São Paulo, SP, Brazil
[d] Instituto de Física de São Carlos, Universidade de São Paulo, São Carlos, SP, Brazil

ARTICLE INFO

Handling Editor: Dr P Colombo

Keywords:
Silver
Bioactive glass
Sol-gel synthesis
Structural characterization

ABSTRACT

Ag-containing bioactive glasses (Ag-BG) have been extensively studied as a bactericidal biomaterial, produced mainly by the sol-gel method over the last decades. According to the literature, sol-gel-derived Ag-BG may show metallic or ionic silver species in the glass structure. However, most of these works lack detailed information about how the addition of silver affects the glass network. In this study, we systematically produced sol-gel derived 58S glasses containing different quantities of Ag_2O (1, 5, and 10 wt%), yielding glasses with different proportions of silver species (Ag^0 or Ag^{+1}). Results from X-ray diffraction and scanning electron microscopy coupled with energy dispersive spectroscopy (SEM-EDS) evidenced the progressive formation of silver crystals due to the addition of silver in the glass structure. ^{29}Si and ^{31}P nuclear magnetic resonance and photoelectronic X-ray spectroscopies evidenced a glass depolymerization caused by Ag^{1+} addition in the glass structure. On the other hand, the presence of silver crystals (Ag^0) removes the network modifier role of silver, yielding glasses with higher network connectivity. A possible mechanism to explain the formation of silver crystals was proposed based on surface nucleation and growth. Finally, we suggest understanding Ag^{1+} or Ag^0 formation as a solution to design glasses with tuned bactericidal properties.

1. Introduction

Bioactive glasses are designed to chemically interact with a host tissue through chemo-physiological reactions, ultimately forming a hydroxyapatite layer. This bioactive layer can chemically bond to the hydroxyapatite from the bone tissue, causing osteointegration between the glass and the host bone. Therefore, these glasses have been extensively applied in orthopedics and odontology, aiming for bone or dental repair and regeneration [1–3]. However, other applications beyond hard tissue are also allowed, as these glasses can bond to soft tissue, thereby being applied in skin wound regeneration and nerve repair [2,4,5].

Bioactive glasses comprise a glass former (like SiO_2, B_2O_3, and P_2O_5) and at least CaO as a glass modifier. Na_2O and K_2O are also commonly found in the glass composition, which means that there are glasses based on binary, ternary, quaternary, or even multicomponent systems [6–9]. Usually, some oxides are added to the glass composition intending to add biological functionalities to the glass structure, also known as therapeutic ions. These ions can display osteogenic, angiogenic, anti-inflammatory, and antibacterial properties, such as zinc (Zn), magnesium (Mg), silver (Ag), strontium (Sr), gallium (Ga), fluor (F), iron (Fe), cobalt (Co), lithium (Li), titanium (Ti) and copper (Cu) [10,11]. However, lanthanides and other transition metals have also been used as less common therapeutic ions [11–13].

Silver is one of the most studied therapeutic ions because of its bactericidal effect, thereby allowing the development of biomaterials that prevent infections, one of the leading causes of implant failure [14]. Besides, Ag-containing bioactive glasses can resurrect the antibiotic effect of antibiotic-resistant bacteria, overcoming a current limitation of the pharmaceutical industry [15]. However, silver is found as Ag^0 or Ag^{1+} species in the glass structure, depending on the chosen processing

* Corresponding author.
E-mail address: juliana.marchi@ufabc.edu.br (J. Marchi).

https://doi.org/10.1016/j.oceram.2023.100449
Received 31 March 2023; Received in revised form 23 August 2023; Accepted 30 August 2023
Available online 1 September 2023

method and synthesis route [16–18]. Consequently, the biological pathways in which Ag^0 and Ag^{1+} species display bactericidal properties differ. The Ag^0 species, mostly found as metallic nanoparticles, kill bacteria through destabilization and rupturing of the cell membrane. On the other hand, the Ag^{1+} species can pass through the bacteria cell membrane and bind to their DNA, blocking their replication, which causes bacteria death [19,20]. In this sense, one can infer that the biological response and efficiency of a bioactive glass doped with silver rely on the presence of Ag^0/Ag^{1+} species, assuming that they might differ in effectiveness.

Although the first Ag-containing bioactive glass dates back to the 2000s [21,22], the reasons why some syntheses yield the formation of Ag^0 or Ag^{1+} are not entirely known. So far, the only control of silver redox reactions can be achieved by thermal treatment, in which a thermal reduction intentionally forms Ag^0 nanocrystals or nanoparticles [16,23–25]. On the other hand, when Ag-containing bioactive glasses are produced by the sol-gel method, some authors have reported the obtainment of metallic silver [15,26], while others reported ionic species [27–32] or even both of them [17].

This work aimed to understand the causes underlying the silver valence criteria in glass networks and the effect of metallic and ionic silver species on their structure. In this sense, we have produced sol-gel-derived 58S bioactive glass compositions ($58SiO_2$–$33CaO$–$9P_2O_5$ wt.%) doped with different silver content, 1, 5, and 10 wt%. Based on our studies, we proposed a mechanism to explain the formation of different silver species and described how their formation affected the glass structure. Understanding the mechanisms underlying silver formation can be a solution to designing more effective antibacterial biomaterials.

2. Materials and methods

2.1. Glass synthesis

Bioactive glasses based on the 58S composition [(100-x) ($58SiO_2$–$33CaO$–$9P_2O_5$)-x(Ag_2O)], wt.%, x = 0, 1, 5, and 10 wt%, were prepared by the quick-alkali sol-gel method [33], and adapted by our research group [12,13,34–36]. These glasses were named BG (x = 0), BG1Ag (x = 1), BG5Ag (x = 5), and BG10Ag (x = 10). Briefly, tetraethyl orthosilicate (TEOS, ≥99%, Sigma Aldrich, Germany) was hydrolyzed for 20 min in a solution containing water, ethanol, and HNO_3 1 M in a 13.9:50: 8 ratio. Then, triethyl phosphate (TEP, ≥99%, Sigma Aldrich, Germany) was added to the mixture for over 20 min. Later, Ca $(NO_3)_2 4H_2O$ (≥99%, Sigma Aldrich, Germany) was added and mixed until complete dissolution. Silver nitrate (99,5%, AgNO3, Sigma-Aldrich, Germany) was added in the Ag-containing glasses after the calcium nitrate tetrahydrate addition. Finally, 10 mL of NH_4OH (28.0–30.0%, Sigma Aldrich, Germany) was quickly dropped into the solution, causing the condensation reaction of silicon species. Then, the resulting gel was dried by freeze drying (Operon, New Zealand) for 48 h.

The glasses synthesized by the sol-gel method were analyzed by differential scanning calorimetry DSC and thermal gravimetric analysis TGA (Setaram, LABSYS evo STA 1600, Switzerland) prior to calcination, aiming to determine their calcination temperature. The analysis was performed from environment temperature up to 1000 °C at a heating rate of 10 °C/min. The calcination temperature was set at 550 °C/1h (EDG 550, Brazil).

2.2. Structural characterization

The amorphous nature of the glasses and possible presence of crystalline phases were analyzed by X-ray diffraction using an X-Ray Diffractometer D8 Focus (AXS Bruker, USA), with CuKα radiation, 40 kV and 40 mA, range of 2Θ angles from 10° to 60°, step size of 0,04°.

Fourier transform infrared spectrophotometer (FTIR, Spectrum Two, PerkinElmer, USA) was used to analyze the vitreous network structure, check the presence of the bridge and non-bridge oxygen functional groups, and verify the formation of new functional groups in the glasses. The analysis was performed in the 500 cm^{-1} to 4000 cm^{-1} spectral window, accumulation of 32 spectra, and a resolution of 4 cm^{-1}.

High-resolution X-ray photoelectron spectroscopy (ThermoFisher, model K alpha+, USA) of Ag3d and O1s spectra was used to analyze the incorporation of silver into the glass structure and calculate the bridging oxygen (BO) and non-bridging oxygen (NBO) ratio in the glass structure. Based on the BO and NBO fractions (denoted $BO_{(O1s)}$ and $NBO_{(O1s)}$, we determined the BO/NBO ratio, as shown in Eq. (1). Also, survey spectra were used to determine the glass network connectivity through the glass composition (in mol %), according to Eq. (2) [37]. The analysis was performed using an Al–K radiation source. In the analysis chamber, the pressure was between 10^{-9} and 10^{-8} mbar, and the X-ray radiation penetrated 10 nm. The spectra calibration was performed using the C1s peak at 284.8 eV. All the collected spectra were analyzed using the software Casa XPS (CallTech, USA).

$$BO/_{NBO} = \frac{BO_{(O1s)}}{NBO_{(O1s)}} \quad \text{Eq.1}$$

$$NBO(XPS) = \frac{4[SiO_2] - 2[CaO + Ag_2O + Na_2O] + 6[P_2O_5]}{[SiO_2]} \quad \text{Eq. 2}$$

The glass structures were also evaluated by solid-state nuclear magnetic resonance (NMR) to verify the effect of silver on the glass network connectivity. The experiments were performed at a magnetic field of 9.4 T in a Varian Unity INOVA spectrometer (USA). The experiments of ^{29}Si-NMR were performed at a magic angle condition of 5 Hz of 7 mm zirconium rotor. A - 5.0 μs was employed as the pulse duration -π/2. The delay cycle was optimized for each sample to guarantee a complete magnetization relaxation. Between 200 and 20000 runs were performed to guarantee a proper signal/noise ratio. A kaolinite sample was used as a secondary standard of chemical shit of Si, with resonance at −1.5 ppm relative to the tetramethylsilane. For ^{31}P NMR single-pulse experiments, powdered samples were spun at 9 kHz at the magic angle condition in 4 mm silicon nitride rotors. The π/2-pulse duration was 2.5 ls. The recycle delay for complete magnetization relaxation varied from 120 to 5 s. The number of scans to get a proper signal-to-noise ratio varied from 380 to 800. A liquid sample of 85% H_3PO_4 was used as a standard for the ^{31}P chemical shift. Based on the ^{29}Si-NMR results, the network connectivity was calculated according to Eq. (3), where x_{Si} denotes the BO fraction of a given Si[Q^n] population, and n is the number of bridging oxygen [38].

$$NC_{NMR} = \sum_n n x_{Si}^n \quad \text{Eq. 3}$$

The microstructure was evaluated by scanning electron microscopy coupled with energy dispersive spectroscopy (SEM-EDS). Before the SEM-EDS analysis, the powders were fixed in carbon tape on metallic supports. Then, the powders were carbon coated (Sputtering Leica EM ACE 200, USA). Morphology and chemical composition of the powder's surface were performed in a scanning electron microscopy JSM-6010LA (JEOL, USA), operating at a 10 kV voltage and a working distance of approximately 10 mm.

3. Results

Initial characterization consists of determining the calcination temperature, thus guaranteeing the complete elimination of nitrates and organic residues from the synthesis and allowing network modifiers to be incorporated into the glass structure. Fig. 1 shows the DSC (left y-axis) and TG (right y-axis) analysis of the BG, BG1Ag, BG5Ag, and BG10Ag glasses. The DSC curves in the BG glass (Fig. 1a) are characterized by five endothermic peaks at 108, 205, 266, 423, and 505 °C. All these endothermic transitions are accompanied by weight loss observed in the TG analysis, which means they are related to degradation or condensation reactions. The first peak at 108 °C involves removing

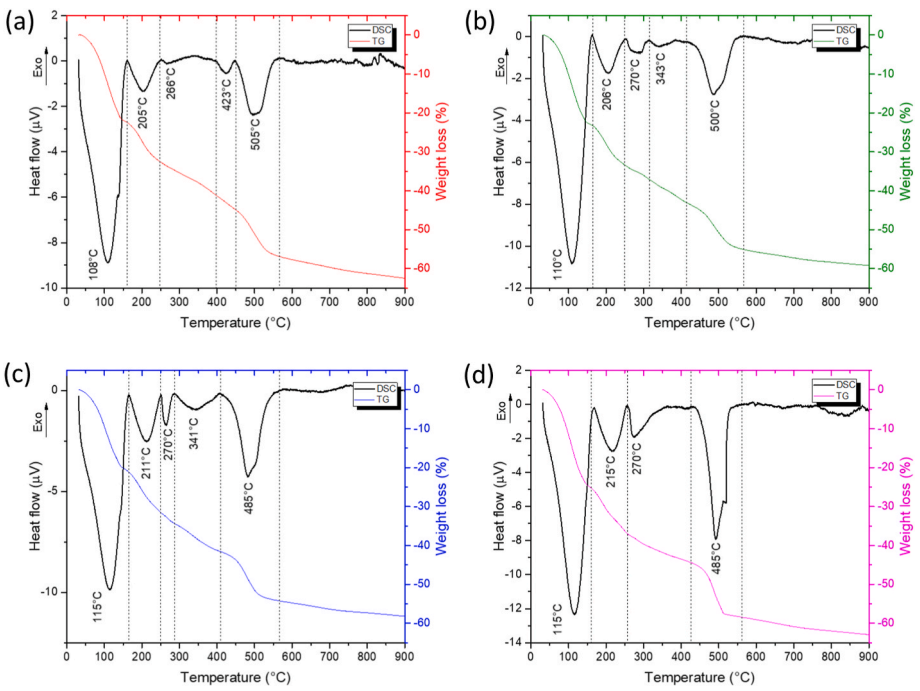

Fig. 1. Differential scanning calorimetry (DSC) and thermal gravimetric TG curves of the BG glass(a) and Ag-containing glasses (b–d) containing 1, 5, and 10% Ag_2O, respectively. The black y-axis on the left displays the DSC analysis's heat flow (μV), while the colored y-axis on the right shows the weight loss (%) of the TG analysis.

water, structural water, and alcohol molecules in the gel powder [33]. Then, the peak at 205 °C is related to the condensation reaction between Si–OH bonds, forming bridging oxygen bonds (Si–*O*–Si) and yielding to H_2O residues, as well as it can be related to the dehydration reaction of calcium nitrates hydrates [39]. The 266 °C and 423 °C peaks possibly relate to residual NH_4NO_3 and HNO_3 thermally removed, respectively,

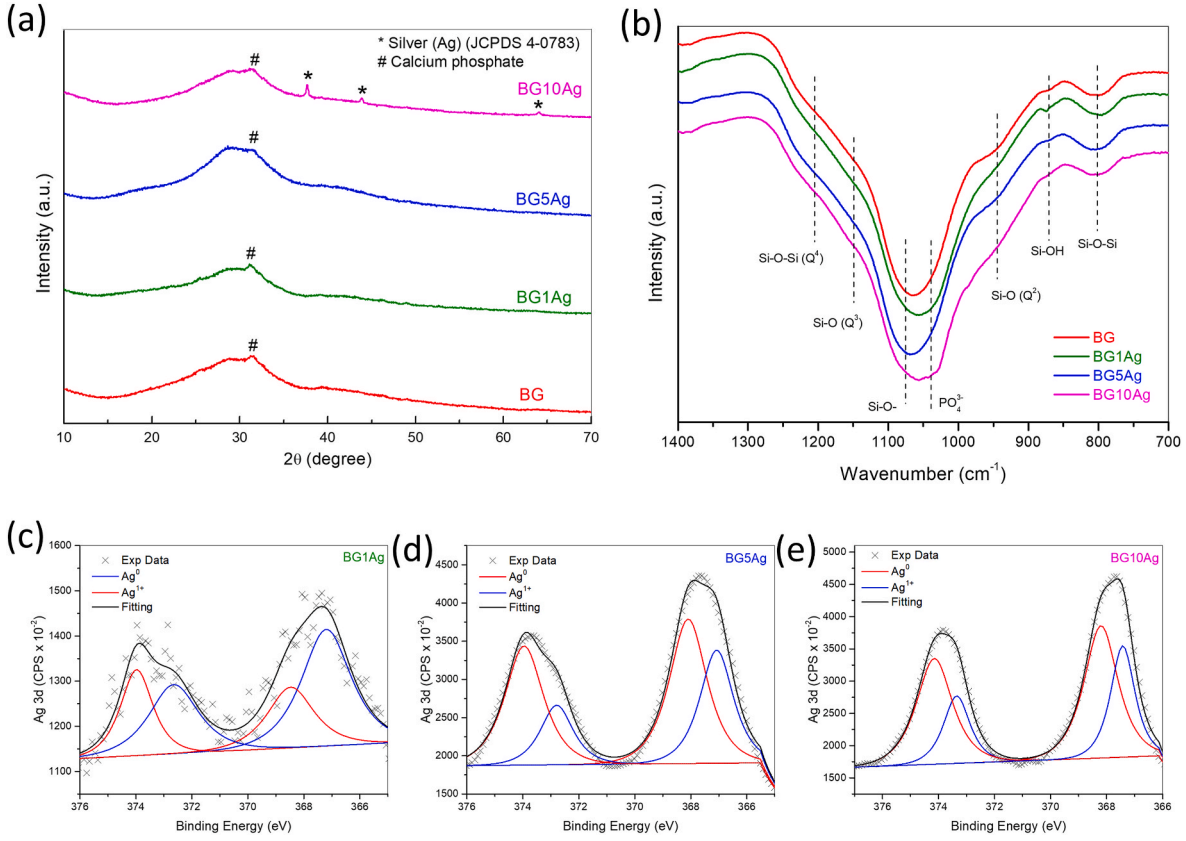

Fig. 2. Structural characterization of the glasses: (a) X-ray diffraction analysis; (b) FTIR spectra; and Ag3d high-resolution XPS spectra of the BG1Ag (c), BG5Ag (d) and BG10Ag (e) glasses.

which could be formed during gel drying. Finally, the peak at 505 °C is related to calcium nitrate decomposition [33,40], the last step before forming the glass network containing the glass formers and modifiers.

Ag-containing glasses (Fig. 1b–d) show thermal behavior similar to the BG glass, that is, five endothermic peaks, from which two are between 110-115 °C and 206–215 °C and another at 270 °C. These three first peaks are similar to those in the Ag-free glass (BG). Then, two more peaks between 341-343 °C and 485–500 °C are also found. The last peak between 485 and 500 °C shows a shoulder nearly at 525 °C. The peak at 423 °C, detected in the BG sample, was not evident in the Ag-BG series, blurred by the subsequent peak at 485–500 °C or lowered its thermal decompositions due to the effect of more nitrates in the synthesis. Finally, the peak between 485 and 500 °C was due to nitrate thermal decomposition. Note that the peak is broader as two nitrate species decompose simultaneously, the calcium nitrate and the silver nitrate [41]. Besides, the shoulder at approximately 525 °C can be associated with a silver thermal reduction [42]. Based on these thermal results, we performed the calcination of the samples at 550 °C/1h to enable residue elimination and the incorporation of the modifiers into the glass network.

After calcination, the glasses were characterized by X-ray diffraction (Fig. 2a), Fourier-transform infrared spectroscopy (Fig. 2b), and X-ray photoelectron spectroscopy (Fig. 2c–e). The quantification of metallic and ionic silver species was performed by Ag 3d peak analysis of the XPS spectra of the BG1Ag (Fig. 2c), BG5Ag (Fig. 2d), and B10Ag (Fig. 2e) glasses.

The XRD diffraction results (Fig. 2a) show that all the glasses were characterized by a broad peak between 20 and 35° related to the short-range ordering of silicon tetrahedrons from the glass structure [43]. A small peak at 32° was noticed in all samples, related to calcium phosphate nanocrystals or clusters found in the glass structure, typical of sol-gel derived bioactive glasses [35,44]. Moreover, peaks at 37 and 48° are also noticed in the BG10Ag glass, related to a crystalline metallic silver phase (JCPDS, no. 4–0783).

Regarding the FTIR results (Fig. 2b), all the glasses showed the same vibrational modes in the observed spectral window. All the vibration modes were related to the glass structure: asymmetric stretching of Si–O bonds (800 cm^{-1}), Si–OH (850 cm^{-1}), stretching of Si–*O*–Si bonds (1060 cm^{-1}), and Q^2 (940 cm^{-1}), Q^3 (1170 cm^{-1}) and Q^4 (1220 cm^{-1}) silicate species [45–47]. The Q^n notation refers to the number (n) of bridging oxygens found in a given silicon tetrahedron.

The fitting of the high-resolution Ag 3d XPS spectra of the Ag-containing glasses (Fig. 2c–e) shows the presence of two different species in all the glasses: Ag^{+1} and Ag^0. However, the amount of Ag^0 increases as more silver is added to the glass composition, suggesting an $Ag^{1+} \rightarrow Ag^0$ redox reaction. The signal/noise ratio was lower in the BG1Ag glass than in the other because of the smaller quantity of silver in its glass composition; fewer photoelectrons were emitted from the sample and detected by the XPS spectrometer detector. Of course, minor errors in the curve fitting may occur with less resolution, but considering the curve shape, it seems that the amount of Ag^0 and Ag^{1+} species in this glass is not a measurement artifact but experimental evidence.

The presence of metallic silver was further confirmed by scanning electron microscopy coupled with energy-dispersive spectroscopy (Fig. 3). Fig. 3a shows the EDS imaging of the glass surfaces, evidencing the homogeneous distribution of Si (green), P (yellow), and Ca (purple) in all the glasses. In the Ag-containing glasses, Ag (cyan) is also homogeneously distributed. Besides, as the Ag_2O content in the glasses shifted from 1 to 10 wt%, an increase in the cyan color's intensity confirms that more silver was incorporated into the glass structure.

As the BG10Ag glass showed the presence of an Ag crystalline phase (as shown in Fig. 2a), an SEM analysis using backscattering electrons was performed in this sample to identify Ag metallic crystals. Fig. 3b shows the SEM micrography of the BG10Ag glass and its EDS mapping of Ag in cyan (Fig. 3c). The Ag^0 crystals are dispersed in the glass structure, which is characterized by brighter points due to the higher electron density of silver. Besides, EDS spectra of the brighter (Fig. 3e) and grey (Fig. 3d) regions also show that the brighter points are indeed Ag^0 crystals due to the more intense peaks of Ag in the EDS spectrum, while the grey regions show an EDS spectrum typical of a 58S glass doped with silver.

The effect of the silver species on the glass network was analyzed by ^{29}Si and ^{31}P NMR (Fig. 4) and high-resolution O1s XPS (Fig. 5). The ^{29}Si-NMR of the BG glass contains a glass network predominantly composed of Q^4 species, preceded by fractions of Q^3 and Q^2. In glasses containing silver up to 5 wt%, glass depolymerization occurs through the formation of Q^1 species in detriment to the decrease in Q^3 and Q^2 ones. It suggests that silver ions (Ag^+) display a glass modifier role in the glass network. However, the ^{29}Si-NMR spectrum of the BG10Ag glass is similar to the BG glass, suggesting a withdrawal of the modifier role of silver in the glass network. A similar trend was noticed in the O1s XPS spectra of the glasses (Fig. 5). Overall, the O1s XPS spectra fitting reveals that all the glasses have a fraction of bridging (BO) and non-bridging oxygen (NBO) species. Comparing the spectra of the BG (Fig. 5a) with the spectra of the BG1Ag (Fig. 5b) and BG5Ag (Fig. 5c) glasses, a decrease in BO species is noticed and accompanied by an increase in NBO, suggesting that the silver behaves mainly as a modifier ion. When the BG5Ag glass is compared with the BG10Ag one (Fig. 5d), there is an increase in BO species, suggesting the withdrawal of silver role as a glass network modifier. The ^{31}P NMR results (Fig. 4b) also emphasize that the BG10Ag favors a phase separation, as the spectra of the BG and BG10Ag glasses show the presence of Q^0 and Q^1, while the BG1Ag and BG5Ag glasses showed only Q^0 species. It highlights that ionic silver was probably interacting with phosphate species and favoring their depolymerization. However, as the BG10Ag predominantly shows metallic silver species, phosphate species polymerize as Q^1 species.

Finally, the role of silver in the glass network connectivity was confirmed by calculating the network connectivity (NC) or the BO/NBO ratio of the glasses by different techniques. Fig. 6 shows the NC of the glasses calculated from the survey XPS spectra of the glasses (red y-axis on the right) and by ^{29}Si-NMR (blue y-axis on the right), as well as their BO/NBO ratio derived from the O1s XPS (black y-axis on the left). In all the cases, the NC or the BO/NBO ratio follows the same trend: a decrease in glass connectivity when silver is added to the glass network, followed by an increase in glass connectivity when the amount of silver in the glass network keeps rising.

4. Discussion

Understanding the mechanism of silver inclusion in the glass network during the sol-gel synthesis supposes that we first need to understand the formation of the glass network of the bioactive glass. Lin et al. [40] described the evolution of the glass network during the sol-gel synthesis of bioactive glasses in five steps: (i) mixing + gelation; (ii) aging; (iii) drying; (iv) stabilization; (v) and sintering. In the first step, the hydrolysis of the glass precursors occurs, with subsequent condensation reaction of the glass network formers (such as TEOS and TEP), leading to the formation of a primary glass particle; besides, these primary particles can bind to other ones through condensation reactions of Si–OH bonds (Eq. (4)), forming secondary particles.

$$Si–OH_{(s)} + OH–Si_{(s)} \rightarrow Si–O–Si_{(s)} + H2O_{(l)} \quad \text{Eq. 4}$$

In the second step, the gelation reaction keeps occurring, but in the quick-alkali method [33], chosen to produce our glasses, this step is unnecessary, as silicon polycondensation reactions occur very fast, consuming the reactants in seconds. Then, in the third step, most of the water from the synthesis is removed by drying either at mild temperatures or freeze drying [34,35]. At this stage, nitrates and calcium ions bind back together, forming calcium nitrates that are deposited on the surface of the secondary particles formed in stage 1. Later, in the fourth stage, as the resulting dried powder is calcined at a temperature near

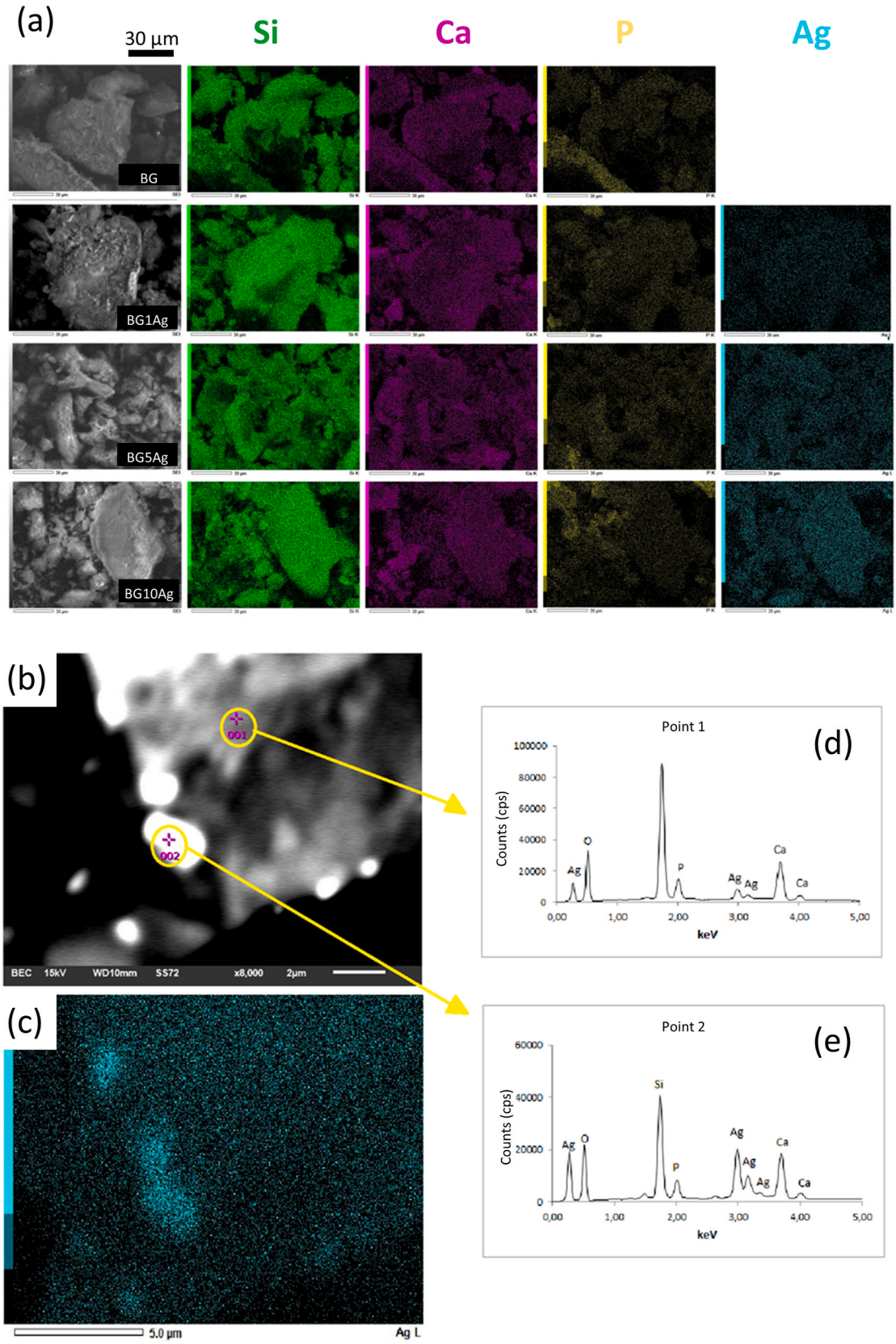

Fig. 3. Scanning electron microscopy of the glasses: (a) EDS mapping of Si (green), Ca (purple), P (yellow), and Ag (cyan) of the BG, BG1Ag, BG5AG, and BG10Ag from top to bottom; (b) backscattered electron microscopy of the BG10Ag glass and its EDS spectra at point 1 (grey, d) and point 2 (brighter, e), as well as its Ag EDS mapping (c). (For interpretation of the references to color in this figure legend, the reader is referred to the Web version of this article.)

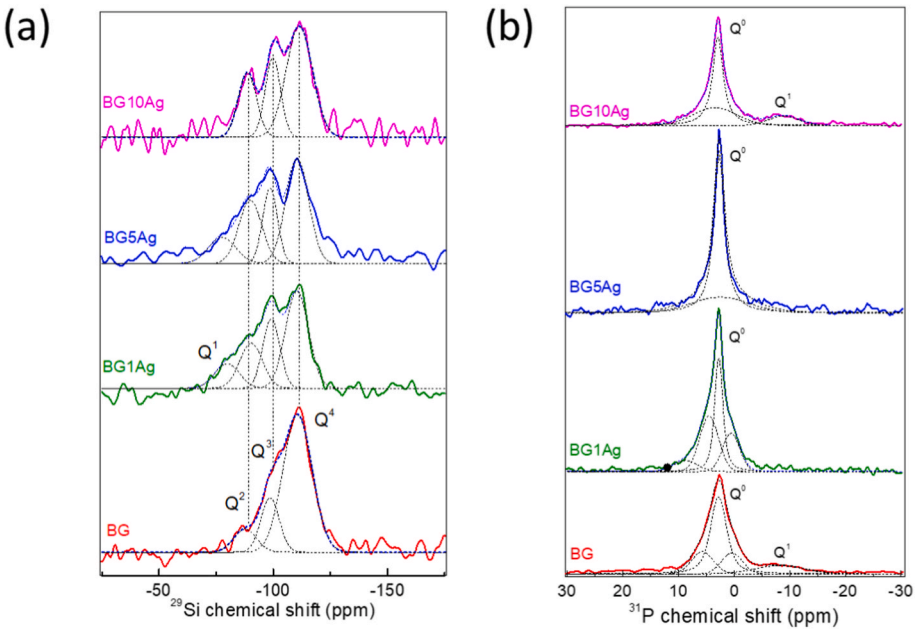

Fig. 4. Nuclear magnetic resonance results: (a) ^{29}Si-NMR and (b) ^{31}P NMR of the BG, BG1Ag, BG5Ag, and BG10Ag glasses.

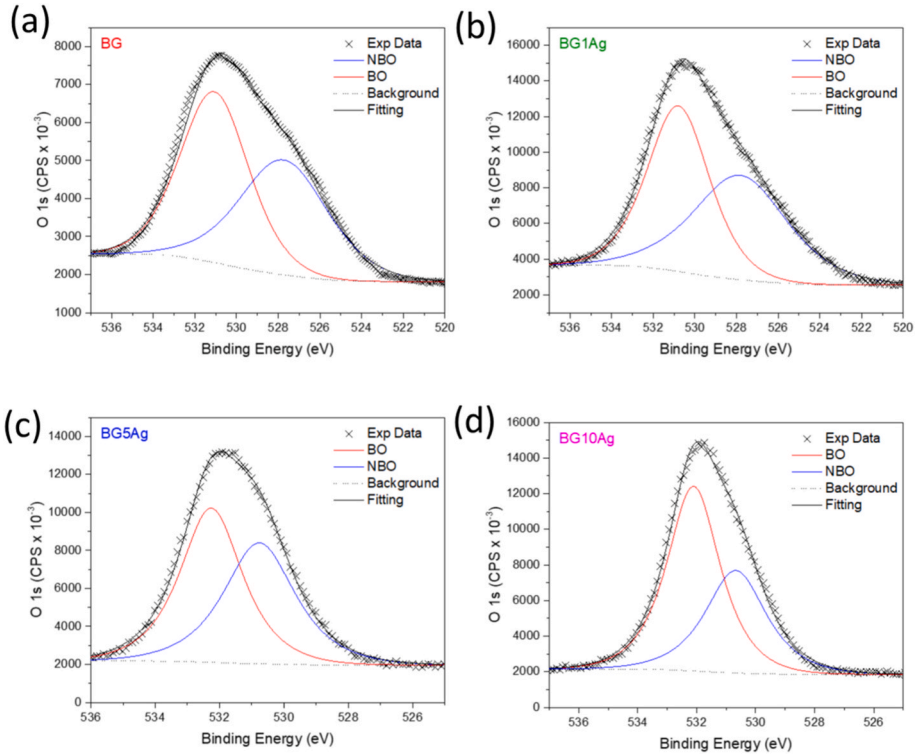

Fig. 5. High-resolution O1s spectra of the developed glasses: (a) BG; (b) BG1Ag; (c) BG5Ag; (d) and BG10Ag.

550 °C, the calcium nitrate is thermally degraded (Eq. (5)). Because the surface of the secondary particles is rich in calcium, the secondary particles reach a glass transition state from the edges to the core of the particles, allowing the diffusion of calcium into the glass network [48]. Therefore, at this stage, there is a decrease in the network connectivity caused by the formation of Si–*O*–Ca bonds. If the temperature keeps increasing, the particles sinter (step 5), forming tertiary particles fused at the corner due to mass flow.

$$2Ca(NO_3)_{2(s)} \rightarrow 2CaO_{(s)} + 4NO_{2(g)}\uparrow + O_{2(g)}\uparrow \quad \text{Eq. 5}$$

The thermal characterization of the glasses (Fig. 1) enables an understanding of the influence of silver on the formation of glass nanoparticles. Overall, Ag-containing glasses behave similarly to Ag-free glasses, except for displaying a more prominent peak related to silver nitrate decomposition and the later thermal reduction of silver. Other works from the literature have also reported the formation of silver by thermal reduction at high temperatures in bioactive glasses [24], which highlights the consistency of our results.

Interestingly, silver species are found as Ag^{+} and Ag^{0} in the glass structure, regardless of the silver content in the glass composition.

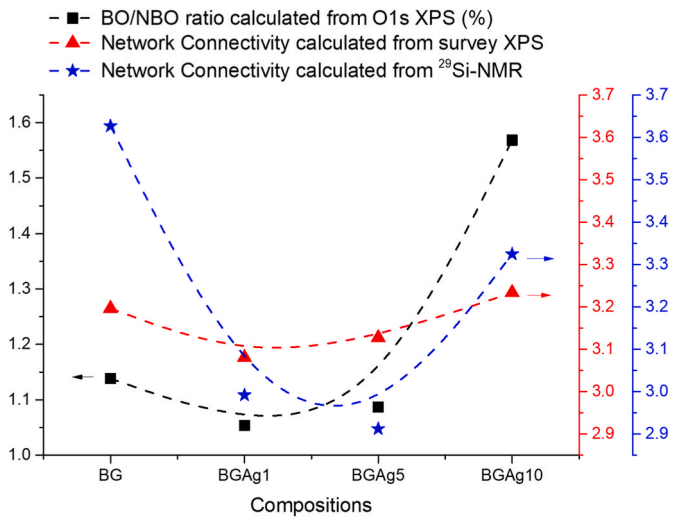

Fig. 6. Effect of silver addition on the glass network of developed glasses: network connectivity (NC) calculated from survey XPS spectra (NC_{XPS}, red triangle); NC calculated from survey ^{29}Si-NMR spectra (NC_{NMR}, blue star); BO/NBO ratio calculated from the high-resolution O1s XPS spectra (black square). (For interpretation of the references to color in this figure legend, the reader is referred to the Web version of this article.)

However, the fraction of Ag^0 increases with the increase in silver content in the glasses, according to Fig. 2c–e. This fact drives us to observe that silver crystals might be present in all Ag-containing glasses, but they were more detectable in the BG10Ag sample (Fig. 2a) as this glass composition has a higher content of silver and, thus, more silver crystals. These results agree with other findings from the literature that have also noticed a formation of silver crystals in their sol-gel bioactive glasses in those glasses that contained a higher fraction of silver in their composition [23,49]. Notably, the production of Ag-containing glasses by the quick alkali method did not favor the crystallization of other phases than silver crystal, which can be an advantage. Other works have reported glass devitrification and the formation of cristobalite, wollastonite, and calcium phosphates [29,49,50]. Since glass devitrification can disfavor bioactivity [48,49], avoiding crystallization can maximize the bactericidal and bioactive properties. Although we noticed some minor calcium phosphate crystals in our glasses (Fig. 2a), they are not a result of glass devitrification but formed during sol-gel synthesis. Recently, it has been reported that TEP has very low hydrolyzation kinetics, and it remains as TEP during all the sol-gel synthesis instead of being found as aqueous phosphate specie. Upon calcination, TEP is degraded, and its affinity to calcium leads to the formation of calcium phosphate domains [51,52]. These calcium phosphates are mostly found as pyrophosphate in the glass structure [52], agreeing with the results of ^{31}P NMR in Fig. 4. Garcia et al. experimentally showed these calcium phosphate domains in sol-gel-derived bioactive glasses through transmission electron diffraction and microscopy [53]. Unlike glass devitrification, forming these calcium phosphate domains does not jeopardize the glass bioactivity, as shown in previous works [34,35].

So far, the results from this work, following the literature's findings, have shown that silver crystals depend on the silver content in the glass compositions. However, it does not clarify the mechanism, that is, whether it is a surface nucleation and growth phenomenon or it is like glass devitrification. The NMR and XPS results (Figs. 4–6) provide evidence of a possible mechanism. Both techniques have shown increased glass network connectivity when the BG5Ag and the BG10Ag glasses are compared, which we addressed to a loss of silver's glass network modifier role. If the formation of silver crystals were driven by glass devitrification, first silver ions would take place in the glass network as glass modifiers and later be crystallized into crystals. In this case, considering that the BG10Ag glass has the double silver content (in wt.%) as the BG5Ag glass, it was reasonable to assume that part of the silver would remain in the glass network, and thus some silicon Q^1 species would be noticed in the ^{29}Si-NMR. Besides, devitrification involves a collaborative mechanism in which the neighbor atoms must re-accommodate, which also favors forming other phases in bioactive silicate glasses, such as silicate crystalline phases [54]. As it does not occur, we suggest silver crystallization is a surface mechanism.

It is worth noting that NC_{NMR} and NC_{XPS} are not the same because the calculus from the chemical composition used from the survey XPS spectra simplifies the complex role of ions with an intermediate role in the glass structure, i.e., act as glass formers and modifiers, like phosphate moieties [38,55,56], neither take into account that part of calcium is crystallized as calcium phosphate, as shown in Fig. 2a. As the NC_{XPS} is derived from the experimental glass compositions, it is less sensitive to the effect of silver segregation from the glass network, as it assumes that all the silver plays a modifier role in the glass structure. The slight variation in the NC as a function of the silver content represents an "ideal" situation where all the silver plays a modifier role. However, the NC calculated from ^{29}Si-NMR and the BO/NBO ratio show that the effect of silver on the glass structure deviates from this ideal situation.

The BO/NBO ratio is much more sensitive to the effect of silver than the NC calculated from survey XPS spectra, as it is calculated from the high-resolution O1s, and it is clear that the addition of silver up to 10 wt % led to a significant increase in the BO/NBO ratio. Then, the NC_{NMR} and the BO/NBO ratio show the same trend. However, while NC_{NMR} varies from 0 to 4, the BO/NBO ratio varies from 0 to 1 because the latter does not consider the fractions of Q^n species but only distinguishes BO from NBO. On the other hand, as NC calculated from ^{29}Si-NMR and BO/NBO ratio shows the same trend, it is reasonable to assume that the effect of silver is an experimental observation.

Besides, when we say that the network modifier role of silver is withdrawn, we are referring to when silver is crystallized into metallic silver nanocrystals; thereby, silver ions are not displaying their modifier role expected by the NC_{XPS}. It does not imply that silver is acting as a glass former. Instead, silver is segregated from the glass structure. By not acting as a glass modifier, the glass structure becomes more connected as fewer modifier ions are present in the glass structure.

Also, as ^{29}Si-NMR is a technique based on the whole sample, while the O1s high-resolution spectra of XPS penetrate only a few nanometers underneath the surface, the ^{29}Si-NMR results are more likely to be more accurate about the glass structure, while the BO/NBO results show a better picture about the glass surface. This instrumental difference can explain why the BO/NBO results are more sensitive to silver crystallization than NC_{NMR}, mainly when 10 wt% of silver is added to the glass composition. XPS data intensify these changes as we propose a mechanism in which silver crystallization happens on the surface rather than within the glass particle.

To facilitate the understanding of this proposed mechanism, we drew a scheme comparing the formation of sol-gel glass particles under three scenarios: i) Ag-free glass, ii) Ag-containing glass with no silver crystals, and iii) Ag-containing glasses with silver crystals (Fig. 7). The first scenario is similar to the mechanism proposed by Lin et al. [40] where primary particles (mainly composed of silicon) form during gelation (polycondensation reaction), which are later agglomerated in bonded through Si–OH condensation reactions during drying. Also, during drying, calcium nitrate is deposited on the secondary particles. Later, when calcined, the particles are fused as calcium nitrates decompose, and calcium diffuses from the surface to the core of the tertiary particle. Scenario II is similar to the first, but silver ions are also deposited on the glass surface besides calcium. After calcination, the silver ions are part of the glass network as glass modifiers. Finally, in scenario III, more silver nitrate is deposited on the glass surface upon drying. The silver nitrate decomposes when the glass is calcined, but the silver ions cluster together instead of diffusing through the glass network. Therefore, they remain on the surface instead of acting as glass modifiers. Fig. 3 shows that the silver crystals are present on the particle surface, giving more

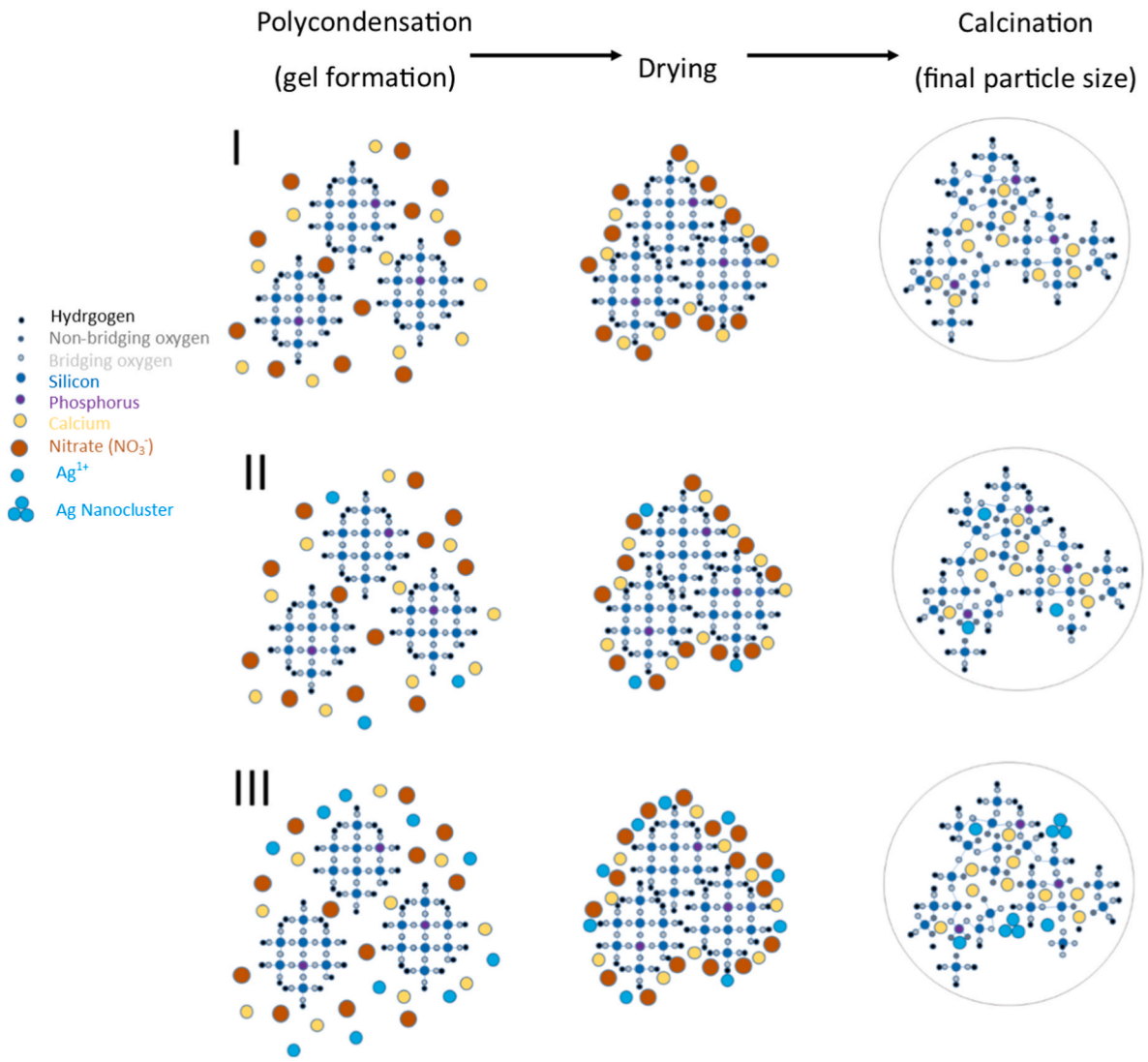

Fig. 7. Schematic illustration of the glass particle formation in different scenarios: I) an Ag-free glass; II) an Ag-containing glass with no silver crystals; III) an Ag-containing glass with silver crystals. In all scenarios, after primary glass particles are formed through the sol-gel synthesis polycondensation reaction, calcium and/or silver nitrates precipitation onto the secondary particles occurs upon drying. Then, when the dried gel is calcined, the nitrates are thermally degraded, and calcium and silver can diffuse to the glass network as mass flow conditions are reached. However, if the concentration of silver reaches a certain level on the glass surface, metallic silver crystals are formed, removing the glass modifier role of silver in the glass network.

evidence of the proposed mechanism. It is worth noting that this crystallization mechanism is not similar to the production of a glass-ceramic, in which a glass is partially crystallized. Instead, this mechanism of silver crystal formation is related to the mechanism of glass particles during the sol-gel synthesis. Indeed, this is the reason why the crystallization occurs at the surface, as shown in Fig. 3.

This proposed mechanism of silver crystal formation in bioactive glasses can be used to tune bactericidal properties. Some authors have addressed that silver ions display higher bactericidal activity than silver nanoparticles [57,58]. Besides, when dispersed in a solid-state matrix, the bactericidal properties of silver nanoparticles rely on their dissolution ability and silver ion release [58,59]. Therefore, designing glasses with modulated Ag^0 or Ag^+ species can be a strategy to tune bactericidal properties, but it depends on precise control of silver species modulation during sol-gel processing.

5. Conclusion

This work produced sol-gel derived 58S bioactive glasses containing 1, 5, and 10 wt% of Ag_2O, obtaining glasses with different ratios of Ag^+ and Ag^0 species. Despite the non-crystalline nature of all glasses, the glass containing the highest concentration of Ag_2O (BG10Ag) showed the formation of metallic silver crystals on its surface. However, Ag3d high-resolution spectra of all Ag-containing glasses showed the presence of Ag^0 and Ag^{1+} species in the glass structure, which means that only the BG10Ag glass had concentrations high enough to get noticeable XRD patterns in the XRD analysis. SEM-EDS analysis proved that metallic silver crystals' nucleation and growth occur on the glass powder's surface. Complimentarily, ^{29}Si and ^{31}P NMR and high-resolution O1s XPS spectra of the glasses suggested that silver ions display a glass modifier role in the glass structure. However, when silver crystals are formed, it removes the network modifier role of silver, reinforcing that metallic silver crystallization occurs on the surface. By understanding the mechanism underlying metallic silver formation in sol-gel bioactive glasses, it might be possible to modulate the bactericidal properties of Ag-containing bioactive glasses, as crystalline silver and ionic silver can display different bactericidal behavior at physiological conditions.

Declaration of interest

The authors declare that they have no known competing financial interests or personal relationships that could have appeared to influence the work reported in this paper.

Acknowledgment

The authors appreciate the facility support from the Central Experimental Multiusuário (CEM) at the Federal University of ABC, as well as the Centro de Ciências e Tecnologia dos Materiais at the Energy and Nuclear Research Institute (CCTM-IPEN), and the Instituto de Física de São Carlos at the University of Sao Paulo (IFSC-USP). The authors also appreciate the financial support provided by the Fundação de Amparo à Pesquisa do Estado de São Paulo (FAPESP) grant no. 20/00329–6and 17/19111–8. This study was financed in part by the Coordenação de Aperfeiçoamento de Pessoal de Nível Superior - Brasil (CAPES) - Finance Code 001.

References

[1] S. Kargozar, F. Baino, S. Hamzehlou, R.G. Hill, M. Mozafari, Bioactive glasses entering the mainstream, Drug Discov. Today 23 (2018) 1700–1704, https://doi.org/10.1016/j.drudis.2018.05.027.

[2] H.R. Fernandes, A. Gaddam, A. Rebelo, D. Brazete, G.E. Stan, J.M.F. Ferreira, Bioactive glasses and glass-ceramics for healthcare applications in bone regeneration and tissue engineering, Materials 11 (2018) 2530, https://doi.org/10.3390/ma11122530.

[3] M. Montazerian, E.D. Zanotto, Bioactive and inert dental glass-ceramics, J. Biomed. Mater. Res. 105 (2016) 619–639, https://doi.org/10.1002/jbm.a.35923.

[4] V. Pal Singh Sidhu, R. Borges, M. Yusuf, S. Mahmoudi, S. Fallah Ghorbani, M. Hosseinikia, P. Salahshour, F. Sadeghi, M. Arefian, A comprehensive review of bioactive glass: synthesis, ion substitution, application, challenges, and future perspectives, Journal of Composites and Compounds 3 (2021) 247–261, https://doi.org/10.52547/jcc.3.4.5.

[5] J. Marchi, Biocompatible Glasses: from Bone Regeneration to Cancer Treatment, first ed., Springer International Publishing, Cham, Switzerland, 2016 https://doi.org/10.1007/978-3-319-44249-5.

[6] P. Saravanapavan, J.R. Jones, R.S. Pryce, L.L. Hench, Bioactivity of gel-glass powders in the CaO-SiO2 system: a comparison with ternary (CaO-P2O5-SiO2) and quaternary glasses (SiO2-CaO-P2O5-Na2O), J. Biomed. Mater. Res. 66 (2003) 110–119, https://doi.org/10.1002/jbm.a.10532.

[7] S.B. Jung, Bioactive borate glasses, Bio-Glasses (2012) 75–95, https://doi.org/10.1002/9781118346457.ch6.

[8] M. Mneimne, R.G. Hill, A.J. Bushby, D.S. Brauer, High phosphate content significantly increases apatite formation of fluoride-containing bioactive glasses, Acta Biomater. 7 (2011) 1827–1834, https://doi.org/10.1016/j.actbio.2010.11.037.

[9] J.K. Christie, R.I. Ainsworth, N.H. De Leeuw, Investigating structural features which control the dissolution of bioactive phosphate glasses: beyond the network connectivity, J. Non-Cryst. Solids 432 (2016) 31–34, https://doi.org/10.1016/j.jnoncrysol.2015.01.016.

[10] A. Hoppe, N.S. Güldal, A.R. Boccaccini, Biomaterials A review of the biological response to ionic dissolution products from bioactive glasses and glass-ceramics, Biomaterials 32 (2011) 2757–2774, https://doi.org/10.1016/j.biomaterials.2011.01.004.

[11] U. Pantulap, M. Arango-Ospina, A.R. Boccaccini, Bioactive glasses incorporating less-common ions to improve biological and physical properties, J. Mater. Sci. Mater. Med. 33 (1) (2021) 1–41, https://doi.org/10.1007/S10856-021-06626-3, 33 (2021).

[12] T. Zambanini, R. Borges, A.C.S. De Souza, G.Z. Justo, J. Machado, D.R. De Araujo, J. Marchi, J. Machado, D.R. De Araujo, Holmium-containing bioactive glasses dispersed in poloxamer 407 hydrogel as a theragenerative composite for bone cancer treatment, Materials 14 (2021) 1459, https://doi.org/10.3390/ma14061459.

[13] G.P. Delpino, R. Borges, T. Zambanini, J.F.S. Joca, I. Gaubeur, A.C.S. de Souza, J. Marchi, Sol-gel-derived 58S bioactive glass containing holmium aiming brachytherapy applications: a dissolution, bioactivity, and cytotoxicity study, Mater. Sci. Eng. C 119 (2021), 111595, https://doi.org/10.1016/j.msec.2020.111595.

[14] T. Zambanini, R. Borges, K.C. Kai, J. Marchi, Bioactive Glasses for Treatment of Bone Infections, 2018, https://doi.org/10.1016/B978-0-08-102196-5.00014-8.

[15] N. Pajares-Chamorro, J. Shook, N.D. Hammer, X. Chatzistavrou, Resurrection of antibiotics that methicillin-resistant Staphylococcus aureus resists by silver-doped bioactive glass-ceramic microparticles, Acta Biomater. 96 (2019) 537–546, https://doi.org/10.1016/j.actbio.2019.07.012.

[16] J.-C. Kung, Y.-J. Chen, Y.-C. Chiang, C.-L. Lee, Y.-T. Yang-Wang, C.-C. Hung, C.-J. Shih, Antibacterial activity of silver nanoparticle (AgNP) confined mesoporous structured bioactive powder against Enterococcus faecalis infecting root canal systems, J. Non-Cryst. Solids 502 (2018) 62–70, https://doi.org/10.1016/j.jnoncrysol.2018.06.030.

[17] C.R. Mariappan, N. Ranga, Influence of silver on the structure, dielectric and antibacterial effect of silver doped bioglass-ceramic nanoparticles, Ceram. Int. 43 (2017) 2196–2201, https://doi.org/10.1016/j.ceramint.2016.11.003.

[18] S. Ferraris, M. Miola, A. Cochis, B. Azzimonti, L. Rimondini, E. Prenesti, E. Vernè, In situ reduction of antibacterial silver ions to metallic silver nanoparticles on bioactive glasses functionalized with polyphenols, Appl. Surf. Sci. 396 (2017) 461–470, https://doi.org/10.1016/j.apsusc.2016.10.177.

[19] J.R. Morones, J.L. Elechiguerra, A. Camacho, K. Holt, J.B. Kouri, J.T. Ramírez, M. J. Yacaman, The bactericidal effect of silver nanoparticles, Nanotechnology 16 (2005) 2346–2353, https://doi.org/10.1088/0957-4484/16/10/059.

[20] S.M. Rabiee, N. Nazparvar, M. Azizian, D. Vashaee, L. Tayebi, Effect of ion substitution on properties of bioactive glasses: a review, Ceram. Int. 41 (2015) 7241–7251, https://doi.org/10.1016/j.ceramint.2015.02.140.

[21] M. Bellantone, L.L. Hench, Bioactive behaviour of sol-gel derived antibacterial bioactive glass, Key Eng. Mater. 192 (195) (2000) 617–620. https://doi.org/10.4028/www.scientific.net/kem.192-195.617.

[22] M. Bellantone, N.J. Coleman, L.L. Hench, A novel sol-gel derived bioactive glass featuring antibacterial properties, Key Eng. Mater. (2000) 597–600, 192–195, https://doi.org/10.4028/www.scientific.net/kem.192-195.597.

[23] J.R.J. Delben, O.M. Pimentel, M.B. Coelho, P.D. Candelorio, L.N. Furini, F. Alencar dos Santos, F.S. de Vicente, A.A.S.T. Delben, Synthesis and thermal properties of nanoparticles of bioactive glasses containing silver, J. Therm. Anal. Calorim. 97 (2009) 433–436, https://doi.org/10.1007/s10973-009-0086-4.

[24] A.C. Marsh, N.P. Mellott, N. Pajares-Chamorro, M. Crimp, A. Wren, N.D. Hammer, X. Chatzistavrou, Fabrication and multiscale characterization of 3D silver containing bioactive glass-ceramic scaffolds, Bioact. Mater. 4 (2019) 215–223, https://doi.org/10.1016/j.bioactmat.2019.05.003.

[25] C. Shuai, Y. Xu, P. Feng, G. Wang, S. Xiong, S. Peng, Antibacterial polymer scaffold based on mesoporous bioactive glass loaded with in situ grown silver, Chem. Eng. J. 374 (2019) 304–315, https://doi.org/10.1016/j.cej.2019.03.273.

[26] S. Naseri, W.C. Lepry, V.B. Maisuria, N. Tufenkji, S.N. Nazhat, Development and characterization of silver-doped sol-gel-derived borate glasses with antibacterial activity, J. Non-Cryst. Solids 505 (2019) 438–446, https://doi.org/10.1016/j.jnoncrysol.2018.11.026.

[27] J.-H. Jung, D.-H. Kim, K.-H. Yoo, S.-Y. Yoon, Y. Kim, M.-K. Bae, J. Chung, C.-C. Ko, Y.H. Kwon, Y.-I. Kim, Dentin sealing and antibacterial effects of silver-doped bioactive glass/mesoporous silica nanocomposite: an in vitro study, Clin. Oral Invest. 23 (2018) 253–266, https://doi.org/10.1007/s00784-018-2432-z.

[28] H.N. Wilkinson, S. Iveson, P. Catherall, M.J. Hardman, A novel silver bioactive glass elicits antimicrobial efficacy against Pseudomonas aeruginosa and Staphylococcus aureus in an ex vivo skin wound biofilm model, Front. Microbiol. 9 (2018) 1450, https://doi.org/10.3389/fmicb.2018.01450.

[29] A.C. Vale, A.L. Carvalho, A.M. Barbosa, E. Torrado, J.F. Mano, N.M. Alves, Novel antibacterial and bioactive silicate glass nanoparticles for biomedical applications, Adv. Eng. Mater. 20 (2017), 1700855, https://doi.org/10.1002/adem.201700855.

[30] F.E. Ciraldo, L. Liverani, L. Gritsch, W.H. Goldmann, A.R. Boccaccini, Synthesis and characterization of silver-doped mesoporous bioactive glass and its applications in conjunction with electrospinning, Materials 11 (2018) 692, https://doi.org/10.3390/ma11050692.

[31] N. Gupta, D. Santhiya, S. Murugavel, A. Kumar, A. Aditya, M. Ganguli, S. Gupta, Effects of transition metal ion dopants (Ag, Cu and Fe) on the structural, mechanical and antibacterial properties of bioactive glass, Colloids Surf. A Physicochem. Eng. Asp. 538 (2018) 393–403, https://doi.org/10.1016/j.colsurfa.2017.11.023.

[32] L. Bunetel, E. Wers, A. Novella, A. Bodin, P. Pellen-Mussi, H. Oudadesse, *In vitro* chemical and biological effects of Ag, Cu and Cu + Zn adjunction in 46S6 bioactive glasses, Mater. Res. Express 2 (2015), 095402, https://doi.org/10.1088/2053-1591/2/9/095402.

[33] W. Xia, J. Chang, Preparation and characterization of nano-bioactive-glasses (NBG) by a quick alkali-mediated sol–gel method, Mater. Lett. 61 (2007) 3251–3253, https://doi.org/10.1016/j.matlet.2006.11.048.

[34] R. Borges, L.M. Ferreira, C. Rettori, I.M. Lourenço, A.B. Seabra, F.A. Muller, E. P. Ferraz, M.M. Marques, M. Miola, F. Baino, J.B. Mamani, L.F. Gamarra, J. Marchi, Superparamagnetic and highly bioactive SPIONS/bioactive glass nanocomposite and its potential application in magnetic hyperthermia, Biomater. Adv. 135 (2022), 112655, https://doi.org/10.1016/j.msec.2022.112655.

[35] R. Borges, L. Mendonça-Ferreira, C. Rettori, I.S.O. Pereira, F. Baino, J. Marchi, New sol-gel-derived magnetic bioactive glass-ceramics containing superparamagnetic hematite nanocrystals for hyperthermia application, Mater. Sci. Eng. C 120 (2021), https://doi.org/10.1016/j.msec.2020.111692.

[36] R. Borges, J. Marchi, Sol-gel synthesis of bioglasses: a growth kinetics study by dynamic light scattering, Adv. Sci. Technol. 102 (2016) 18–23. https://doi.org/10.4028/www.scientific.net/AST.102.18.

[37] R.G. Hill, D.S. Brauer, Predicting the bioactivity of glasses using the network connectivity or split network models, J. Non-Cryst. Solids 357 (2011) 3884–3887, https://doi.org/10.1016/j.jnoncrysol.2011.07.025.

[38] R. Mathew, B. Stevensson, A. Tilocca, M. Edén, Toward a rational design of bioactive glasses with optimal structural features: composition-structure correlations unveiled by solid-state NMR and MD simulations, J. Phys. Chem. B 118 (2014) 833–844, https://doi.org/10.1021/jp409652k.

[39] A. Zhao, B. Xiong, Y. Han, H. Tong, Thermal decomposition paths of calcium nitrate tetrahydrate and calcium nitrite, Thermochim. Acta 714 (2022), 179264, https://doi.org/10.1016/j.tca.2022.179264.

[40] S. Lin, C. Ionescu, K.J. Pike, M.E. Smith, J.R. Jones, Nanostructure evolution and calcium distribution in sol-gel derived bioactive glass, J. Mater. Chem. 19 (2009) 1276–1282, https://doi.org/10.1039/B814292k.
[41] S.F. Etris, Silver and silver alloys, in: Kirk-Othmer Encyclopedia of Chemical Technology, John Wiley & Sons, Inc., 2001, https://doi.org/10.1002/0471238961.1909122205201809.a01.pub2.
[42] J.R.J. Delben, O.M. Pimentel, M.B. Coelho, P.D. Candelorio, L.N. Furini, F. Alencar Dos Santos, F.S. De Vicente, A.A.S.T. Delben, Synthesis and thermal properties of nanoparticles of bioactive glasses containing silver, J. Therm. Anal. Calorim. 97 (2009) 433–436, https://doi.org/10.1007/s10973-009-0086-4.
[43] B.E. Warren, X-ray diffraction study of the structure of glass, Chem Rev 26 (1940) 237–255, https://doi.org/10.1021/CR60084A007/ASSET/CR60084A007.FP.PNG_V03.
[44] I. Izquierdo-Barba, A.J. Salinas, M. Vallet-Regí, Bioactive glasses: from macro to nano, Int. J. Appl. Glass Sci. 4 (2013) 149–161, https://doi.org/10.1111/ijag.12028.
[45] S.A. MacDonald, C.R. Schardt, D.J. Masiello, J.H. Simmons, Dispersion analysis of FTIR reflection measurements in silicate glasses, J. Non-Cryst. Solids 275 (2000) 72–82, https://doi.org/10.1016/s0022-3093(00)00121-6.
[46] M.M. Pereira, A.E. Clark, L.L. Hench, Calcium phosphate formation on sol-gel-derived bioactive glassesin vitro, J. Biomed. Mater. Res. 28 (1994) 693–698, https://doi.org/10.1002/jbm.820280606.
[47] J. Serra, P. González, S. Liste, C. Serra, S. Chiussi, B. León, M. Pérez-Amor, H. O. Ylänen, M. Hupa, FTIR and XPS studies of bioactive silica based glasses, J. Non-Cryst. Solids 332 (2003) 20–27, https://doi.org/10.1016/j.jnoncrysol.2003.09.013.
[48] E.M.R. Lee, R. Borges, J. Marchi, C. de Paula Eduardo, M.M. Marques, Bioactive glass and high-intensity lasers as a promising treatment for dentin hypersensitivity: an in vitro study, J. Biomed. Mater. Res. B Appl. Biomater. 108 (2020) 939–947, https://doi.org/10.1002/jbm.b.34446.
[49] A. Vulpoi, L. Baia, S. Simon, V. Simon, Silver effect on the structure of SiO2-CaO-P2O5 ternary system, Mater. Sci. Eng. C 32 (2012) 178–183, https://doi.org/10.1016/j.msec.2011.10.015.
[50] A.W. Wren, A. Coughlan, P. Hassanzadeh, M.R. Towler, Silver coated bioactive glass particles for wound healing applications, J. Mater. Sci. Mater. Med. 23 (2012) 1331–1341, https://doi.org/10.1007/s10856-012-4604-8.
[51] O.M. Vargas Machuca Bueno, M.A. San-Miguel, C.A. Bertran, E. Zacarias da Silva, J.H. Lopes, Unveiling the mechanism of the triethyl phosphate hydrolysis reaction in the synthesis of the sol-gel-derived 58S bioactive glass, Mater. Today Chem. 24 (2022), 100929, https://doi.org/10.1016/j.mtchem.2022.100929.
[52] O.M.V.M. Bueno, C.L. Herrera, C.A. Bertran, M.A. San-Miguel, J.H. Lopes, An experimental and theoretical approach on stability towards hydrolysis of triethyl phosphate and its effects on the microstructure of sol-gel-derived bioactive silicate glass, Mater. Sci. Eng. C 120 (2021), 111759, https://doi.org/10.1016/j.msec.2020.111759.
[53] A. García, M. Cicuéndez, I. Izquierdo-Barba, D. Arcos, M. Vallet-Regí, Essential role of calcium phosphate heterogeneities in 2D-hexagonal and 3D-cubic SiO2−CaO−P2O5 mesoporous bioactive glasses, Chem. Mater. 21 (2009) 5474–5484, https://doi.org/10.1021/cm9022776.
[54] A. Pedone, V. Cannillo, M.C. Menziani, Toward the understanding of crystallization, mechanical properties and reactivity of multicomponent bioactive glasses, Acta Mater. 213 (2021), 116977, https://doi.org/10.1016/j.actamat.2021.116977.
[55] M. Edén, The split network analysis for exploring composition-structure correlations in multicomponent glasses: I. Rationalizing bioactivity-composition trends of bioglasses, J. Non-Cryst. Solids (2011), https://doi.org/10.1016/j.jnoncrysol.2010.11.098.
[56] R. Mathew, B. Stevensson, M. Edén, Na/Ca intermixing around silicate and phosphate groups in bioactive phosphosilicate glasses revealed by heteronuclear solid-state NMR and molecular dynamics simulations, J. Phys. Chem. B 119 (2015) 5701–5715, https://doi.org/10.1021/acs.jpcb.5b01130.
[57] W.-R. Li, T.-L. Sun, S.-L. Zhou, Y.-K. Ma, Q.-S. Shi, X.-B. Xie, X.-M. Huang, A comparative analysis of antibacterial activity, dynamics, and effects of silver ions and silver nanoparticles against four bacterial strains, Int. Biodeterior. Biodegrad. 123 (2017) 304–310, https://doi.org/10.1016/j.ibiod.2017.07.015.
[58] A. Hamad, K.S. Khashan, A. Hadi, Silver nanoparticles and silver ions as potential antibacterial agents, J. Inorg. Organomet. Polym. Mater. 30 (2020) 4811–4828, https://doi.org/10.1007/s10904-020-01744-x.
[59] L. Wang, G. Periyasami, A. Aldalbahi, V. Fogliano, The antimicrobial activity of silver nanoparticles biocomposite films depends on the silver ions release behaviour, Food Chem. 359 (2021), 129859, https://doi.org/10.1016/j.foodchem.2021.129859.